Capillary-Force-Induced Formation of Luminescent Polystyrene/(Rare-Earth-Doped Nanoparticle) Hybrid Hollow Spheres

Min Chen,[†] Lin Xie,[†] Fuyou Li,[†,§] Shuxue Zhou,[†] and Limin Wu*[,†,§]

Department of Materials Science, Department of Chemistry, and Advanced Materials Laboratory, Fudan University, Shanghai 200433, P. R. China 200433

ABSTRACT This paper presents a "one-pot" procedure to synthesize polystyrene/(rare-earth-doped nanoparticles) (PS/REDNPs) hybrid hollow spheres via the in situ diffusion of organic core into inorganic shell under strong capillary force. In this approach, when carboxyl-capped PS colloids were deposited by different REDNPs in aqueous medium, such as LaF_3:Eu^{3+}, LaF_3:Ce^{3+}-Tb^{3+}, and YVO_4:Dy^{3+}, PS/REDNPs inorganic−organic hybrid hollow spheres could be directly obtained via the in situ diffusion of core PS chains into the voids between rare-earth-doped nanoparticles through the strong capillary force. Not only is the synthetic procedure versatile and very simple, but also the obtained hybrid hollow spheres are hydrophilic and luminescent and could be directly used in chemical and biological fields.

KEYWORDS: hybrid • hollow spheres • rare-earth-doped nanoparticles • capillarity force • luminescence • hydrophilic

Synthesis of monodisperse hollow spheres is currently attracting continuous interest because these hollow spheres have potential applications in catalysis, photonic crystal, chromatography, protection of biologically active agents, fillers (or pigments, coatings), and dye-sensitized solar cells (1−3). In particular, the hollow spheres composed of rare-earth-doped nanoparticles are of interest recently not only because of their diverse properties, such as high quantum yield, low photobleaching, narrow emission bands, and long luminescent lifetimes, as compared with conventional luminescent materials, but also because these luminescent hollow spheres could be used as carrier of targeted drugs for bioapplications (4). For instance, Liang et al. (4b) fabricated PEG/rare-earth hybrid microcapsules via a modified Kirkendall effect process. In their method, glycol served as both solvent and reactant and coordinated with the lanthanide to form an ethylene glycol precursor. Then HNO_3-oxidized product of glycol, such as oxide and/or formic acid readily coordinated with rare earth ions to form insoluble rare earth hydroxides. Polymerization between the ligands and solvent promoted by HNO_3 under solvothermal conditions could further stabilize the product and lead to the formation of inorganic−organic hybrid capsules. Jia et al. (4d) prepared well-shaped Y_2O_3:Eu hollow microspheres via a urea-based homogeneous precipitation technique in the presence of colloidal carbon spheres as hard templates followed by a subsequent heat treatment process. Guan et al. obtained rare earth phosphate hollow spheres via an Ostwald ripening process (4e). These preparation processes are attractive, however, some evident defects, such as cumbersome and time-consuming physical and chemical processes in templates is insurmountable, whereas Kirkendall effect and Ostwald ripening techniques are primarily limited to specific materials such as metals, metal oxides, and chalcogenides (including Au, Ag, platinum−cobalt oxides). And moreover, the as-obtained pure rare-earth hollow spheres are easily fragmented because of their poor mechanical property. Furthermore, the as-obtained luminescent materials always suffer from the drawback of hydrophobic surface ligands (such as oleic acid, oleic amine, or linoleic acid) (5), which could not meet the current demand for bioapplications.

Herein, we report for the first time a facile and versatile method for fabrication of organic−inorganic hybrid hollow spheres with polystyrene/rare-earth-doped nanoparticles as hybrid shell by the aid of capillary force. The detailed preparation procedure is schematically described in Scheme 1. First, carboxyl-capped polystyrene (PS) particles were synthesized and then deposited by rare-earth-doped nanoparticles (REDNPs) (LaF_3:Eu^{3+}, LaF_3:Ce^{3+}-Tb^{3+}, or YVO_4:Dy^{3+}) through the strong interaction between carboxyl or carbonyl groups with the REDNPs (6). During this deposition or later, the PS chains diffused from core particles into the voids between rare-earth-doped nanoparticles under capillary force, forming an organic−inorganic hybrid shell and directly yielding PS/REDNPs hybrid hollow spheres. Compared with previous stretagies, our method is facile and versatile, one can fabricate different PS/REDNPs hybrid hollow spheres by simply changing the host and the activator ions of the nanoparticles. And the obtained hybrid hollow spheres are robust because of the existence of macromo-

* Corresponding author. E-mail: lmw@fudan.edu.cn or lxw@fudan.ac.cn.
Received for review August 13, 2010 and accepted August 30, 2010
† Department of Materials Science, Fudan University.
‡ Department of Chemistry, Fudan University.
§ Advanced Materials Laboratory, Fudan University.
DOI: 10.1021/am100726w

Scheme 1. Schematic Diagram for the Formation of PS/REDNPs Hybrid Spheres

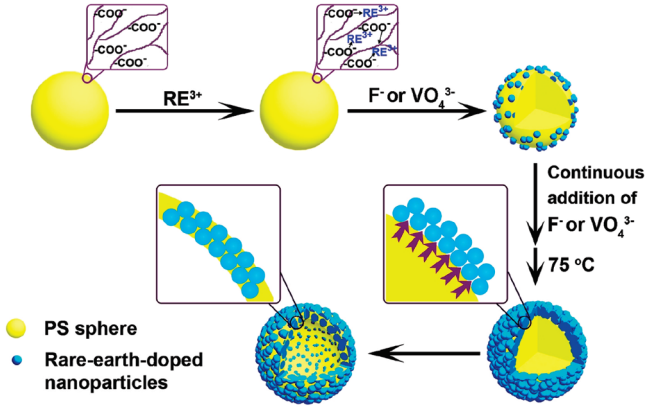

lecular chains in the shell, and highly hydrophilic, which could be directly used in chemical and biological fields.

Figure 1 presents the typical TEM and SEM images of the PS/REDNPs hybrid hollow spheres using PS colloids with the diameter of 280 nm as the template. After deposition of REDNPs, the resultant spheres exhibit rough surfaces in despite of different hosts and rare earth ions doped and the diameters increased to 340 nm. More interestingly, the strong contrast between the dark ring and the pale center indicates a uniform hollow structure (Figure 1a–c). The typical PS/LaF_3:Eu^{3+} hybrid spheres were further scanned by SEM, which shows a monodisperse size and rough surface (Figure 1e). The artificially broken PS/LaF_3:Eu^{3+} hybrid spheres unveils an obvious cavity in the center (Figure 1f), which can further confirm the hollow structure of these

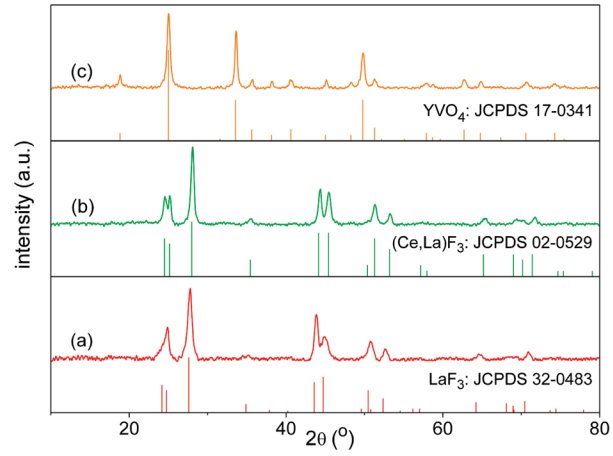

FIGURE 2. XRD patterns of the as-synthesized PS/REDNPs hybrid spheres: (a) PS/LaF_3:Eu^{3+}, (b) PS/LaF_3:Ce^{3+}-Tb^{3+}, (c) PS/YVO_4:Dy^{3+}, as well as the standard data for hexagonal LaF_3 (JCPDS 32−0483), hexagonal (Ce, La)F_3 (JCPDS 02−0529), and tetragonal YVO_4 (JCPDS 17−0341).

hybrid spheres. The XRD patterns of these hollow spheres, as shown in Figure 2, display characteristic peak positions, which have good agreement with the data for the host crystals, indicating that the REDNPs have crystallized well and the breadth of the diffraction peaks distinctly reveals that the sizes of REDNPs are 11−14 nm based on the Scherrer equation.

Selected PS/LaF_3:Eu^{3+} hybrid spheres as well as pure PS spheres were examined with TGA analysis (see the Supporting Information, Figure S1). Compared with the weight loss of pure PS colloids mainly occurring between 350 and 450 °C, the pyrolysis of hollow spheres occurs within the same

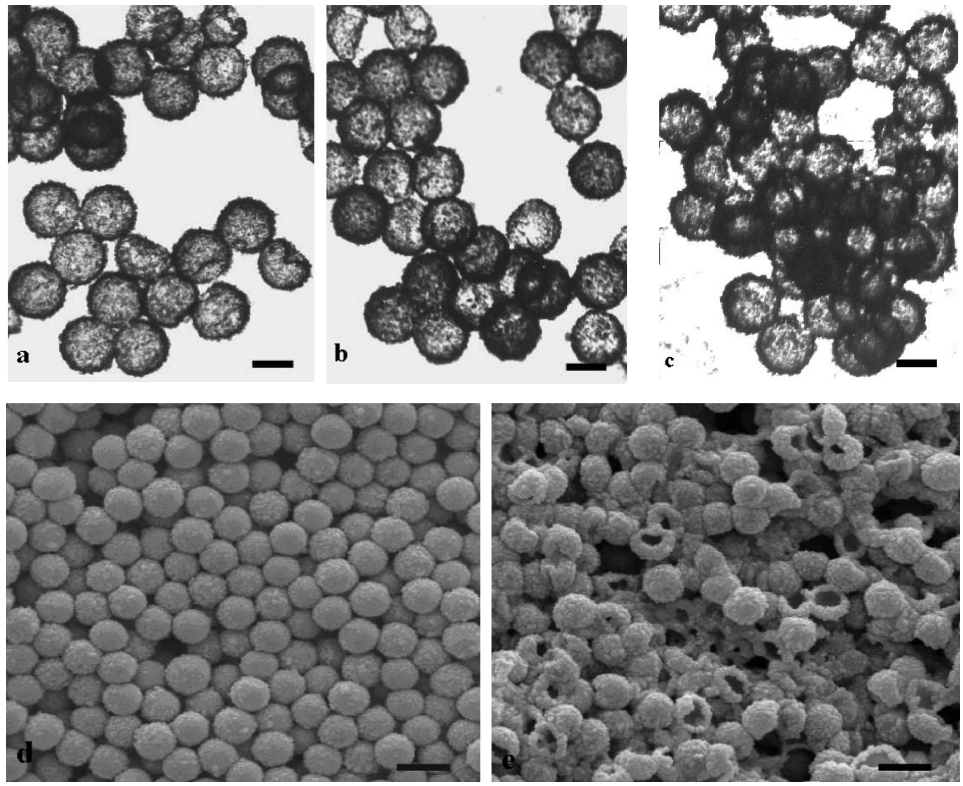

FIGURE 1. Typical TEM images of (a) PS/LaF_3:Eu^{3+}, (b) PS/LaF_3:Ce^{3+}-Tb^{3+}, (c) PS/YVO_4:Dy^{3+}; typical SEM image of (d) PS/LaF_3:Eu^{3+}, (e) artificially broken PS/LaF_3:Eu^{3+} hollow spheres. The scale bars are 250 (a–d) and 500 nm (d, e), respectively.

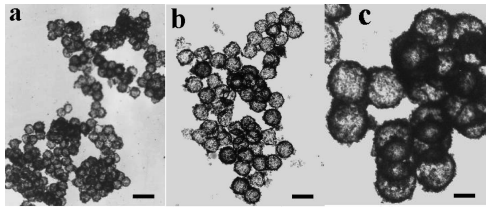

FIGURE 3. TEM images PS/LaF_3:Eu^{3+} hybrid hollow spheres with various diameters of template particles: (a) 80, (b) 150, (c) 410 nm; the scale bars are 250 nm.

temperature region but with about 54% of residue. This is assumed to be pure LaF_3:Eu^{3+}, and has a good agreement with the theoretical weight percentage of LaF_3:Eu^{3+} (58%) according to the feed ratio. This can validate that the as-obtained hollow spheres are composed of PS and RED-NPs, both of them constitute an organic−inorganic hybrid shell.

PS colloids with the average diameters of 80, 150, and 410 nm were also used as templates, the corresponding PS/LaF_3:Eu^{3+} hollow spheres with an average diameter of 110, 200, and 500 nm were obtained, respectively, as shown in Figure 3. This means that the size of hybrid hollow spheres can be easily tuned by adjusting the diameters of templates to meet the demand for bioapplications. However, when the size of PS colloids increased to 1.2 μm, hollow structures could be rarely observed. This was probably because the templates were too large to completely migrate into the voids between LaF_3:Eu^{3+} nanoparticles.

On the basis of the above results and discussion, we deduce the formation mechanism of the PS/LaF_3:Eu^{3+} hybrid hollow spheres as follows. After addition of $LaCl_3$ into PS dispersion, the La^{3+} ions adsorb on the surfaces of PS particles because of the coordination between carboxyl and La^{3+} ions, and LaF_3:Eu^{3+} nanoparticles form immediately after addition of NaF solution because LaF_3 has a very small solubility product constant ($K_{sp} = 2.0 \times 10^{-19}$ at 25 °C) (7a). At a certain concentration of La^{3+} ions, the surfaces of PS particles are compactly covered by LaF_3:Eu^{3+} nanoparticles. Because the PS domain has much lower surface free energy than LaF_3:Eu^{3+} nanoparticles, and the T_g of polymer could be lower in water (7b), the non-cross-linked PS chains can move freely under large capillary force caused by the voids of LaF_3:Eu^{3+} nanoparticles, diffusing from PS particles into the voids between inorganic nanoparticles to reduce the surface energy of the whole system, hence directly forming hollow structure. This capillary-force-induced migration of polymer chains is similar as the previous MIMIC (microfluidic lithography or micromolding in capillaries) process, whose operation principle was based on the capillarity-induced filling of channels by polymers (8). Herein, the concentration of the La^{3+} ions and the reaction temperature are the key factors to form well-defined hollow structure. Insufficient concentration of La^{3+} ions would lead to a thin shell of inorganic particles which can be easily deformed during the diffusion of polymer chains, intact hollow spheres can only be obtained at 0.8 mmol of La^{3+} or above (see the Supporting Information, Figure S2). Low temperature would not make PS chains move easily, and hence hollow spheres could not

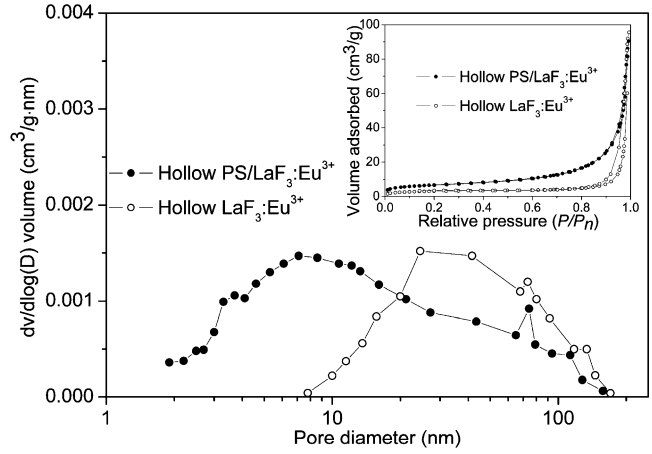

FIGURE 4. Pore size distribution curves and nitrogen adsorption and desorption isotherms (inset) of the LaF_3:Eu^{3+}/PS hybrid hollow spheres and LaF_3:Eu^{3+} hollow spheres after etching by THF.

be formed (see the Supporting Information, Figure S3). To confirm this mechanism, we used a cross-linked PS template as control, which caused raspberry-like PS/LaF_3:Eu^{3+} spheres rather than hollow spheres. On the basis of this mechanism, other PS/REDNPs hybrid hollow spheres, such as PS/LaF_3:Ce^{3+}-Tb^{3+} and PS/YVO_4:Dy^{3+}, can also be obtained by changing the activator ions and even by altering the host materials. And this method can also be used to synthesize PS/SiO_2 or PS/Ag hybrid hollow spheres by simply replacing the rare-earth-doped nanoparticles with SiO_2 or Ag nanoparticles (see the Supporting Information, Figure S4). Therefore, this process can be regarded as a facile and versatile method to fabricate various organic−inorganic hybrid hollow spheres, as long as the capillary force between the closely packed inorganic nanoparticles is large enough to induce the migration of the PS chains.

This formation mechanism can be further confirmed by BET result, as shown in Figure 4. The BET surface areas of the hybrid spheres and the LaF_3:Eu^{3+} hollow spheres (etching the PS ore by THF) are 18.1 and 11.3 m^2/g, and the average pore sizes are 23.2 and 52.5 nm, respectively. The decrease in BET surface area and the increase in average pore size should be attributed to the filled voids between LaF_3:Eu^{3+} by polymer chains.

Figure 5a displays the excitation and emission spectra of the PS/LaF_3:Eu^{3+} hybrid hollow spheres. The characteristic absorption bands of Eu^{3+} can be seen from the energy levels $^5D_4$ at 361 nm, $^5G_6$ at 376 nm, $^5G_2$ at 380 nm, $^5L_6$ at 397 nm, $^5D_3$ at 414 nm, $^5D_2$ at 464 nm. The excitation spectrum is dominated by the $^7F_0 \rightarrow {}^5L_6$ transition of Eu^{3+} at about 397 nm. The emission spectrum is mainly located in the red spectral region, and the characteristic Eu^{3+} transition can be seen from the excited $^5D_1$ at $^5D_0$ levels to ^7F_J ($J = 0-4$) levels (9a). Besides Eu^{3+} ion, Ce^{3+} and Tb^{3+} ions were codoped into the LaF_3 nanocrtystals, in which Ce^{3+} absorbs light and transfer energy to Tb^{3+}. The excitation spectrum of PS/LaF_3:Ce^{3+}-Tb^{3+} hybrid spheres, as indicated in Figure 5b, is exclusively composed of the excitation of Ce^{3+}, which corresponds to the adsorption of the 4f → 4f5d bands of Ce^{3+}. The emission spectrum reveals the typical emission bands

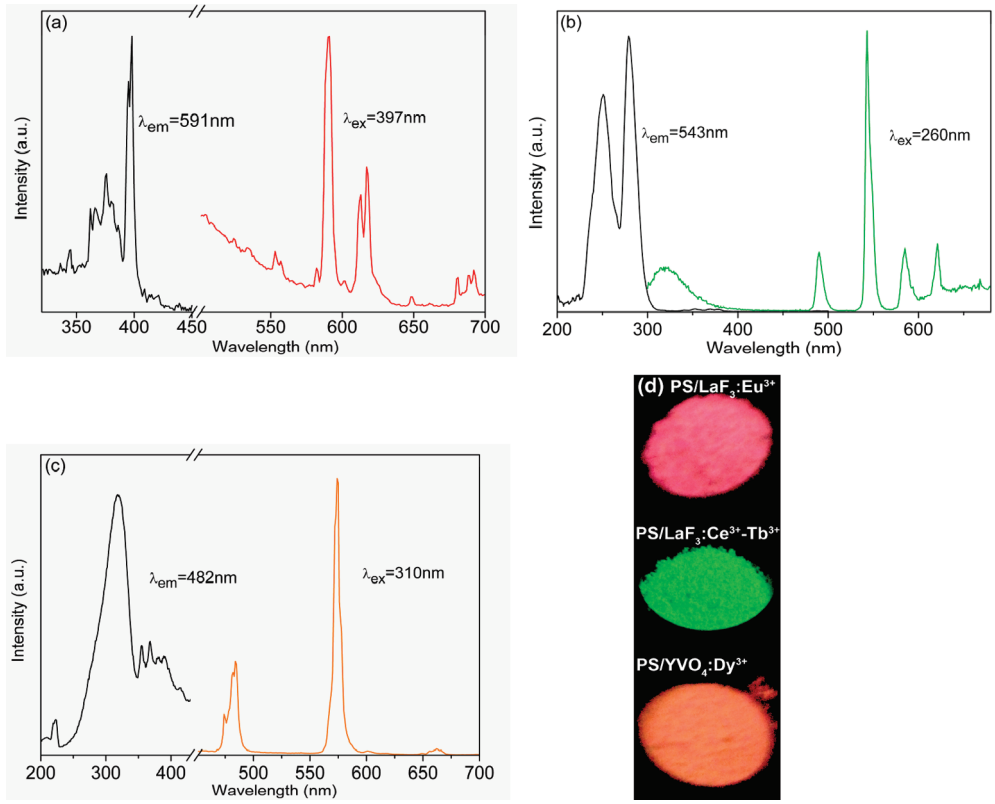

FIGURE 5. Excitation (left) and emission (right) spectra of PS/REDNPs hybrid hollow spheres (a) PS/LaF_3:Eu^{3+}, (b) PS/LaF_3:Ce^{3+}-Tb^{3+}, (c) PS/YVO_4:Dy^{3+} in aqueous solution, and (d) the corresponding luminescence photographs of the spheres powders under 254 nm excitation.

of the $^5D_4 \rightarrow {}^7F_J$ ($J = 6-3$) transition of Tb^{3+} between 450 and 700 nm, and an emission band of Ce^{3+} at 325 nm that is not completely quenched, can be observed (9b). The excitation spectrum of PS/YVO_4:Dy^{3+} hybrid spheres, as shown in Figure 5c, consists of a strong absorption band centered at 310 nm and some weak lines in the longer wavelength region. The strong broad band is due to the absorption of VO_4^{3-} groups, which is attributed the charge transfer from the oxygen ligands to the central vanadium ions inside the VO_4^{3-} groups (9c). The weak lines in the longer wavelength region are due to the f−f transitions (356 nm: $^6H_{15/2} \rightarrow {}^6P_{7/2}$; 370 nm: $^6H_{15/2} \rightarrow {}^6P_{5/2}$; 391 nm: $^6H_{15/2} \rightarrow {}^6M_{21/2}$) of Dy^{3+} within its $^4F_9$ configuration (9d). Excitation into the vanadate groups at 310 nm yields the characteristic emission of Dy^{3+} in the blue region with a maximum at 482 nm and yellow region with a maximum at 573 nm (Figure 5c). These bands correspond to the $^4F_{9/2} \rightarrow {}^6H_{15/2}$ transition and $^4F_{9/2} \rightarrow {}^6H_{13/2}$ transition of Dy^{3+} ions, respectively. Moreover, the emission band of VO_4^{3-} is not observed, indicating that the energy transfer from the vanadate groups to Dy^{3+} is complete. The luminescence photographs of these three hybrid spheres under UV lamp show red, green, and orange colors, respectively (Figure 5d), indicating that these samples possess good emission colors.

In summary, this communication presents a novel and facile method for synthesis of PS/REDNCs hybrid hollow spheres through the induction of capillary force. On the basis of this approach, various PS/REDNCs hybrid hollow spheres along with several other organic−inorganic hybrid hollow spheres can be synthesized. The obtained hybrid hollow spheres are hydrophilic and robust, which can be used in chemical and biological sensors and medicine-based devices.

Acknowledgment. Financial support of this research from the National Natural Science Foundation of China (50903019), National "863" Foundation, the Foundation for the Author of National Excellent Doctoral Dissertation of PR China (200943), the Shanghai Rising-Star Program (10QA1400300), and the innovative team of Ministry of Education of China (IRT0911) are appreciated.

Supporting Information Available: Experimental section, selected TEM images, and TGA results (PDF). This material is available free of charge via the Internet at http://pubs.acs.org.

REFERENCES AND NOTES

(1) (a) Yin, Y.; Rioux, R. M.; Erdonmez, C. K.; Hughes, S.; Somorjai, G. A.; Alivisators, A. P. *Science* **2004**, *304*, 711–714. (b) Wang, W.; Zhen, L.; Xu, C.; Chen., J.; Shao, W *ACS Appl. Mater. Interfaces* **2009**, *1*, 780–788.

(2) (a) Wang, Y.; Cai, L.; Xia, Y. *Adv. Mater.* **2005**, *17*, 473–477. (b) Wang, Y.; Xia, Y. *Nano Lett.* **2004**, *4*, 2047–2050. (c) Lan, Y.; Yang, L.; Zhang, M.; Zhang, W.; Wang, S. *ACS Appl. Mater. Interfaces.* **2010**, *2*, 127–133.

(3) (a) Lee, H.; Char, K. *ACS Appl. Mater. Interfaces.* **2009**, *1*, 913–920. (b) von Werne, T.; Patten, T. *J. Am.Chem. Soc.* **2001**, *123*, 7497–7505. (c) Chen, M.; Wu, L.; Zhou, S.; You, B. *Adv. Mater.* **2006**, *18*, 801–806. (d) Wang, Z.; Wu, L.; Chen, M.; Zhou, S. *J. Am. Chem. Soc.* **2009**, *131*, 11276–11277.

(4) (a) Carmen, I.; Zoldesi, N.; Imhof, A. *Adv. Mater.* **2005**, *17*, 924–928. (b) Liang, X.; Xu, B.; Kuang, S. M.; Wang, X. *Adv. Mater.* **2008**, *20*, 3739–3744. (c) Mayers, B.; Jiang, X.; Sunderland, D.; Cattle, B.; Xia, Y. *J. Am. Chem. Soc.* **2003**, *125*, 13364–13365. (d) Jia, G.; Song, Y.; You, H.; Zhang, H. *Cryst. Growth Des.* **2009**, *1*, 301–307.

(e) Guan, M.; Tao, F.; Sun, J.; Xu., Z. *Langmuir* **2008**, *24*, 8280–8283.

(5) (a) Li, P.; Peng, Q.; Li, Y. *Adv. Mater.* **2009**, *21*, 1945–1948. (b) Mai, H.; Zhang, Y.; Si, R.; Yan, Z.; Sun, L.; You, Y.; Yan, C. *J. Am. Chem. Soc.* **2006**, *128*, 6426–6436. (c) Wang, X.; Zhuang, J.; Peng, Q.; Li, Y. *Nature* **2005**, *437*, 121–124.

(6) (a) Liu, T.; Yang, Y.; Duan, G,.; Gao, Y.; Zeng, Z. *J. Appl. Polym. Sci.* **2009**, *112*, 3388–3394. (b) Huignard, A.; Buissette, V.; Laurent, G.; Gacoin, T.; Boilot, J. *Chem. Mater.* **2002**, *14*, 2264–2269.

(7) (a) Brown, T.; LeMayJr, H.; Bursten, B. *Chemistry—The Central Science*, 8th ed.; Prentice-Hall International: Upper Saddle River, NJ, 2000; p 1023. (b) Song, M.; Hourston, D.; Silva, G.; Machado, J *J. Polym. Sci., Part B: Polym. Phys.* **2001**, *39*, 1659–1664.

(8) (a) Kim, E.; Xia, Y.; Whitesides, G. M. *Nature.* **1995**, *376*, 581–584. (b) Zhang, Y.; Sun, X.; Si, R.; You, L.; Yan, C. *J. Am. Chem. Soc.* **2005**, *127*, 3260–3261.

(9) (a) Stouwdam, J.; van Veggel, F *Nano Lett.* **2002**, *2*, 733–737. (b) Zhu, X.; Zhang, Q.; Li, Y.; Wang, H. *J. Mater. Chem.* **2008**, *18*, 5060–5062. (c) Yu, M.; Lin, J.,; Wang, Z; Fu, J.; Wang, S.; Zhang, H.; Han, Y. *Chem. Mater.* **2002**, *14*, 2224–2231. (d) Shen, W.; Pang, M.; Lin, J.; Fang, J. *J. Electrochem. Soc.* **2005**, *152*, 25–28.

AM100726W